Rheol Acta (2014) 53:333–347
DOI 10.1007/s00397-014-0764-4

ORIGINAL CONTRIBUTION

Fluctuations in flow produced by competition between apparent wall slip and dilatancy

Ryan J. Larsen · Jin-Woong Kim · Charles F. Zukoski · David A. Weitz

Received: 30 March 2013 / Revised: 2 February 2014 / Accepted: 10 February 2014 / Published online: 16 March 2014
© Springer-Verlag Berlin Heidelberg 2014

Abstract Dense suspensions can exhibit a dramatic stress-induced transition from liquid-like to solid-like behavior. In many materials, the solid-like flow state is characterized by large flow fluctuations and instabilities. Although various experiments have been performed to characterize flow fluctuations, the mechanisms that govern the flow instabilities remain poorly understood. To elucidate these mechanisms, we characterize a system that rapidly fluctuates between two flow states. One of the flow states is dominated by apparent wall slip, and the other is dominated by dilatancy. The dilatant regimeoccurs at elevated stresses and is associated with reduced wall slip, whereas the wall slip-dominated regime occurs at lower stresses. At stresses that are intermediate between these two regimes, the material fluctuates between the two regimes in a semi-regular fashion. Our analysis of the fluctuations at millisecond timescales shows that fluctuations occur because neither regime is capable of supporting a constant stress in a stable manner. We rationalize our results in terms of the differences in the shear-induced particle pressure between regions that are particle-rich and regions of slip that are particle-depleted.

Keywords Shear thickening · Dilatancy · Wall slip · Normal stress · Slip velocity · Flow fluctuations

R. J. Larsen (✉) · J.-W. Kim · D. A. Weitz
School of Engineering and Applied Sciences, Harvard University, 29 Oxford St., Cambridge, MA 02138, USA
e-mail: larsen@illinois.edu

R. J. Larsen · C. F. Zukoski
Department of Chemical and Biomolecular Engineering, University of Illinois at Urbana-Champaign, 114 Roger Adams Lab, 600 South Mathews, Urbana, IL 61801, USA

J.-W. Kim
Department of Applied Chemistry, Hanyang University, 55 Hanyangdaehak-ro, Sangnok-gu, Ansan, Gyeonggi-do, 426–791, Korea

D. A. Weitz
Department of Physics, Harvard University, 29 Oxford St., Cambridge, MA 02138, USA

Present Address:
R. J. Larsen
Beckman Institute, 405 N. Matthews, Urbana, IL 61801, USA

Present Address:
C. F. Zukoski
Office of the Provost, The State University of New York at Buffalo, 562 Capen Hall, Buffalo, NY 14260, USA

Introduction

Dense particulate suspensions commonly exhibit a dramatic stress-induced transition from liquid-like to solid-like behavior. In the solid-like state, the material resists flow; this can increase pumping costs, interfere with processing operations, and even damage machinery (Barnes 1989). However, the solid-like state can also be useful for body armor (Lee et al. 2003) and industrial granule formation and provide cohesive effects during materials processing and cleanup (Cates et al. 2005; Barnes 1989). Many of these applications exploit the fact that the solid-like behavior emerges only when stress is applied and the material is flowing. However, the flowing materials are difficult to characterize because they often exhibit significant fluctuations and instabilities (Franks et al. 2000; Larsen et al. 2010; Lootens et al. 2003; Laun et al. 1991). The instabilities are a manifestation of the paradoxical nature of these "flowing solids"; however, the mechanisms that govern the fluctuation are not well understood.

Flow fluctuations are associated with the formation of clusters of particles. One proposed mechanism for cluster formation is the onset of hydrodynamic forces, which gives rise to effective attractions between particles (Bossis and Brady 1989; Bender and Wagner 1995, 1996). A defining feature of shear thickening driven by hydrodynamic forces is the presence of a negative first normal stress difference, N_1,this feature has been observed in simulations and experiments (Lee et al. 2006; Laun 1994; Foss and Brady 2000). However, hydrodynamical effects do not account for shear thickening in materials that exhibit dilatancy, which is manifested as a positive normal force (Brown and Jaeger 2012) or a positive N_1 (Fall et al. 2008). Dilatancy is a manifestation of frictional contact forces between particles that cause an outward expansion of the particle phase (Brown and Jaeger 2012). This mechanism is particularly relevant for suspensions at high concentrations. In this regime, crowding, or jamming, effects can become significant, and the flow behavior is governed by the proximity of the suspension to a critical volume fraction that is close to random close packing (Brown and Jaeger 2009; Kramb et al. 2010) In this regime, the solid-like characteristics of the material become especially pronounced: cracks can appear on the surface of the liquid, and large globules of solid-like material can be formed (Franks et al. 2000; O'Brien and Mackay 2000; Waitukaitis and Jaeger 2012). Under these conditions, particle confinement can be severe, and the particles accommodate deformation by pushing each other outwards, as if to expel them from the suspension (Fall et al. 2010; Lootens et al. 2005). The dilating particles can deform the liquid-air interface of the material, thereby giving it a matted appearance (Cates et al. 2005). The forces required to obtain this deformation are provided by jammed networks of particle-particle contacts (Cates et al. 1998; Melrose and Ball 2004). Because the material is flowing, these networks are transient in nature,their formation and break up may give rise to variety of time-dependent flow effects. Observed time-dependent effects in shear thickening materials include hysteresis, thixotropy, and a metastable high shear rate before a precipitous drop in shear rate at the onset of shear thickening (Laun et al. 1991). The solid-like nature of the shear-induced structures is further underscored by the observations of long relaxation times after the cessation of flow (O'Brien and Mackay 2000; D'Haene et al. 1993). Fluctuating flows during shear thickening have been characterized using standard rheological experiments performed under both controlled shear rate and controlled stress conditions (Frith and Lips 1995; Larsen et al. 2010; Lootens et al. 2003, 2005; Boersma et al. 1991; Laun et al. 1991). In the stress-controlled experiments, suspensions commonly exhibit discontinuous shear thickening: the suspension remains fixed at a constant mean apparent shear rate even as the applied stress varies over a wide range of values. The magnitude of the fluctuations, characterized by the standard deviation of the apparent shear rate, also remains fixed for the same range of stress values (Larsen et al. 2010). These parameters characterize a material state that depends only on the volume fraction, rather than the applied stress. As the volume fraction increases, both of the parameters decrease such that their ratio remains constant,both reach zero at a critical volume fraction that is close to random close packing (Fall et al. 2012; Kramb et al. 2010). In this state, the material is a jammed solid,it can support a wide range of stress without flow because all of the particles are immobilized by stress-bearing contacts with neighboring particles (Kramb and Zukoski 2011; Bertrand et al. 2002). As the volume fraction decreases below the critical volume fraction, the system continues to support stresses in an elastic fashion,for stresses that are sufficiently large, no flow is possible without fluctuations (Larsen et al. 2010).

Although fluctuations are a common feature of dilatant flow, little is known about the mechanism that produces them. Fluctuations in shear-thickened flows have been modeled with elastic elements subject to yielding during homogeneous flow (Head et al. 2002). However, direct observations have revealed nonhomogeneous flow effects, including slip and shear banding (Brown and Jaeger 2012; Boersma et al. 1991; Yilmazer and Kalyon 1991). Rapid particle migration gives rise to a nonuniform distribution of particles (Fall et al. 2010), and inhomogeneities can give rise to temporal fluctuations (Nakanishi et al. 2012; Nakanishi and Mitarai 2011). Regular flow fluctuations have recently been observed in pressure-driven flows of dense suspensions in narrow microchannels (Isa et al. 2009) and in gravity-driven particulate flows through constriction geometry (Kulkarni et al. 2010). These fluctuations likely result from periodic compaction and rarefication of dense clusters of particles and are accommodated by the alternating flows of the solvent into and out of the clusters. However, interpretation of the results from channel flows is complicated by the fact that the stresses at the wall are not directly measured. By contrast, standard rheometers can measure both shear and normal stresses at the boundary of the material. Examination of the oscillating flows with these experiments has the potential to characterize the dynamical stresses that arise during the transient fluctuations in the flow (Lootens et al. 2003, 2005).

Here, we examine the transient stresses associated with regular oscillations of a shear thickening material. Transient stresses during fluctuations are obtained from precision measurements of angular velocity and acceleration during a constant stress experiment in a rheometer. A plot of the instantaneous shear stress in the sample as a function of the apparent shear rate reveals that the material oscillates between two distinct flow regimes: one that is characterized by apparent near-Newtonian flow behavior and the other by

dilatancy. Our ability to distinguish between these regimes over millisecond timescales allows us to perform a slip analysis that pertains only to the near-Newtonian regime. The viscosity correction shows that within this regime, the true macroscopic flow curve is not near-Newtonian, but rather shear thickening. Although apparent wall slip is significant in this regime, the magnitude of the slip is dramatically reduced as the material enters the dilatant regime. These results show that the completing effects of dilatancy and wall slip can produce significant flow fluctuations because neither state is capable of supporting an applied stress in a steady manner.

Experimental

We present results obtained from additional analysis of experiments that have previously been described in detail (Larsen et al. 2010). Our material consists of homemade polystyrene particles that are dispersed in an aqueous solution containing 0.05 wt.% Pluronic® F-68 surfactant (Fluka) (Kim et al. 2007). Here, we present results obtained using uniform spherical particles of diameter 5.8 ∝m; similar results were obtained with nonspherical particles of similar size.

For each set of particles, we first prepare a dilute stock solution. We measure the mass fraction of the particles by weighing a drop of a sample before and after moderate heating to remove all solvent. The concentrated samples are obtained from stock solution by gentle centrifugation and removal of supernatant. The mass fraction of each of the concentrated solutions is calculated based on the mass of the removed solvent and the measured mass fraction of the stock solution. The weight fractions of the concentrated solution are converted to volume fractions by assuming that the density of the polystyrene particles is 1.05 g/mL, and that the density of the suspending liquid is 1 g/mL.

Rheological characterization of the suspensions is performed using parallel plate geometry on a stress-controlled rheometer (AR-G2, TA Instruments). This geometry is used so that we can characterize flow inhomogeneity by collecting data at various gap heights. The gap height is determined by the amount of liquid loaded onto the lower plate. The sample is loaded into the geometry by gently spooning it onto the lower plate. The upper plate is gradually lowered, while gently rotating, until the sample completely fills the gap between the plates. No excess material is removed from the geometry. This gives rise to some variability in the height of the gap; however, comparisons between samples of different volume fraction, φ, are compared only when the gap heights, d, vary by no more than 10 %. A solvent trap connected using vacuum grease is used to prevent drying. To reduce slip, plates of roughened and parylene-coated aluminum are attached to both the upper and lower plates provided by the manufacturer.

Rheological characterization is performed by shearing the sample between the plates. The lower plate remains stationary, and the upper plate is rigidly connected to a shaft that is rotated by a motor that provides a constant torque. The torque is converted to a stress, σ, by using the standard proportionality constant for the parallel plate geometry. An optical encoder measures the rate of the rotation of the upper plate, and this is proportional to an apparent shear rate, $\dot{\gamma}_{\mathrm{app}}$. The material response is then characterized in terms of an apparent viscosity, given by $\eta_{\mathrm{app}} = \sigma/\dot{\gamma}_{\mathrm{app}}$.

Results

Low stress: reproducible shear thickening

The initial experiment consists of a series of ascending σ values from 0.1 to 45 Pa, following by a series of descending and identical σ values. Each value of σ is applied for 10 s. The apparent shear rate is calculated by averaging measurements of the rate of rotation over the final 5 s, after the sample has achieved a steady rate of rotation. Values of η_{app} calculated from the initial ascending series of stress values are usually higher than values of η_{app} measured during the subsequent descending series. However, in most samples, the latter values are consistent with the values of η_{app} measured during a second and identical series of ascending and descending steps in σ. In these cases, measurements of a reproducible flow curve indicate that a steady state has been established (see square and diamond symbols in Fig. 1). The exception to this occurs in spherical particles at highest φ, $\varphi = 0.594$, for which the flow curves are less reproducible (see triangle symbols in Fig. 1). Despite these differences, all samples exhibit shear thickening in the approximate range of 1 Pa $< \sigma <$10 Pa, followed by a plateau in η_{app} in the range of 10 $< \sigma <$45 Pa (see Fig. 1(a)).

The elevated values of η_{app} during the initial stress ramp are likely due to shear-induced aggregation during the loading of the sample. The solid-like behavior is removed, and the sample returned to a low-viscosity state by shear at the moderate stresses near 45 Pa. This gentle shear breaks up the aggregates and establishes a reproducible state in which identical flow curves are obtained during repeated measurements in both the up and down directions. The tendency of our samples to form shear-induced aggregates increases with φ; for the spherical particles of highest φ, shown in Fig. 1, the shear-induced structure is persistent; gentle shear at 45 Pa is not sufficient to return the sample to a liquid-like state. Our observations of a persistent, yet reversible, shear-thickened state are consistent with those of previous reports (Bertrand et al. 2002; Cates et al. 2005).

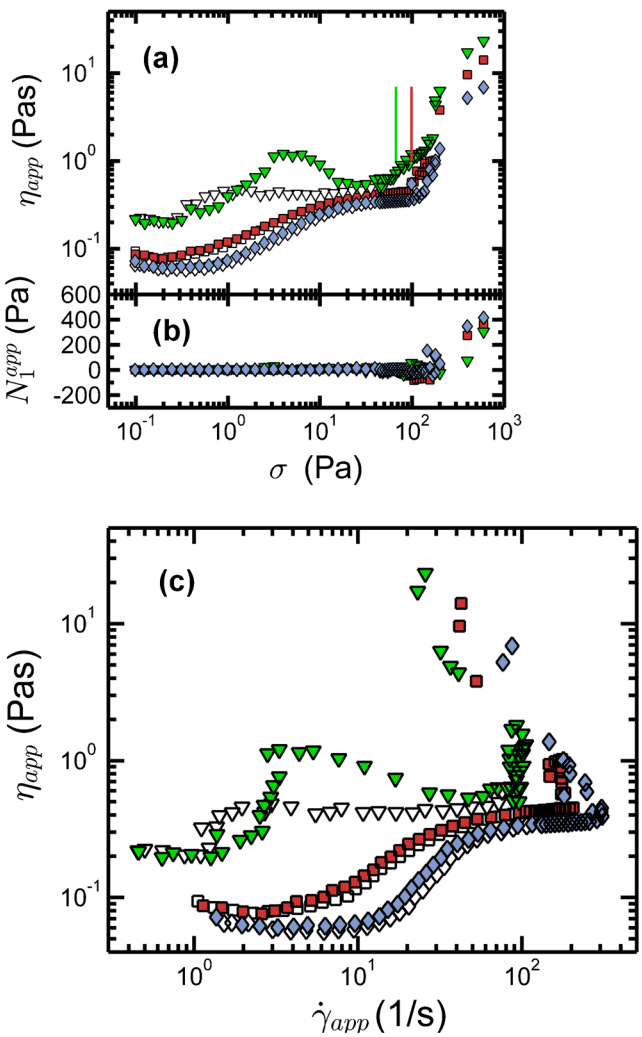

Fig. 1 (Color online) Flow curves from stress-controlled experiments. Values of (**a**) η_{app} and (**b**) N_1^{app} tend to increase with σ, revealing shear thickening and dilatancy, respectively. (**c**) A plot of η_{app} as a function of $\dot{\gamma}_{\text{app}}$ reveals discontinuous shear thickening. Data are shown for spherical particles at volume fraction φ = 57.3 % (*diamonds*, gap height, d = 1,050 ∝m), φ = 58.3 % (*squares*, d = 950 ∝m), φ = 59.4 % (*triangles*, d = 1,000 ∝m). For 0.1 Pa $< \sigma <$ 45 Pa, data points from are taken from the second series of ascending (*closed symbols*) and descending (*open symbols*) stress steps performed after the loading of the sample. This regime exhibits gradual shear thickening. A subsequent series of ascending stress steps (*solid symbols*) between σ = 45 Pa and σ_c (*vertical lines*) reveal a regime of more extreme shear thickening, or dilatancy. The dilatant regime persists to higher stresses, as revealed by step stress tests at 200, 400, and 600 Pa (*solid symbols*)

Because some of our samples exhibit irreversible changes in η_{app} during the experiments, we are careful to perform the same experiments on all samples in the same order and with the same timing parameters. Comparisons between samples are obtained by comparing experiments performed at similar time points. This is particularly important for comparing experiments at higher values of σ where more solid-like behavior is observed.

Moderate stress: onset of solid-like behavior

The transition to solid-like behavior is probed with series of ascending steps in σ beginning at $\sigma = 45$ Pa. Each value of σ is applied for 6 s, and values of $\dot{\gamma}_{\text{app}}$ are calculated by averaging the rate of rotation during the final 4 s of the stress step. These measurements show a continuation of the plateau in η_{app} until σ reaches a critical value, σ_c, where there is a second increase in η_{app}. For the spherical particles shown in Fig. 1, $\sigma_c = 99$ Pa for $\varphi = 57.3$ and 58.3 %, and $\sigma_c = 67$ Pa for $\varphi = 59.4$ % (shown by the vertical lines in Fig. 1(a)).

Near this transition, we visually observe large fluctuations in the rate of rotation of the upper plate. For some samples, not shown here, we removed the solvent trap to directly observe the sample. In this regime, the surface of the sample becomes more matted and solid-like in appearance (O'Brien and Mackay 2000; Cates et al. 2005; Brown and Jaeger 2012) In some samples, generally those consisting of spherical particles, cracks form on the surface of the sample, and portions of the sample churn out of the rheometer (Franks et al. 2000). To avoid significant irreversible changes in the sample, the experiment is stopped after several data points are acquired at $\sigma > \sigma_c$ in the solid-like regime.

High stress: solid-like flow

We then perform a different type of experiment to probe material properties at values of σ that are significantly higher than σ_c. This consists of a series of stress steps in which σ is varied in a regular pattern of 200, 400, 200, and 600 Pa. Each value of σ is applied for approximately 2 s, and the pattern is repeated four times. By probing the values $\sigma = 400$ and 600 Pa rapidly, we are able to minimize the irreversible changes to the sample due to the high stresses. Moreover, by frequently returning to the same values of σ throughout the experiment, we are able to monitor the severity of the time-dependent changes and to distinguish them from the σ-dependent changes. Because significant fluctuations are present in this regime, a high sampling rate of the angular position is necessary for accurate measurements of angular velocity. We resolve the fluctuations in time by monitoring the angular displacement at a rate of 250 points per second, using a raw data collection tool provided by the manufacturer of the rheometer (Larsen et al. 2010). A backward derivative of this data is used to calculate an apparent shear rate, $\dot{\gamma}_{\text{app}}$. We then calculate an average apparent shear rate, $\bar{\dot{\gamma}}_{\text{app}}$, by averaging $\dot{\gamma}_{\text{app}}$ over the entire σ step. We also calculate an apparent viscosity, η_{app}, for each σ step, from the ratio $\sigma/\bar{\dot{\gamma}}_{\text{app}}$. For clarity of presentation, we plot in Fig. 1 only the values of η_{app} from the first series of stress steps that consists of the pattern 200, 400, 200, and

600 Pa. The trends that are apparent from this data are similar to those observed when we plot data obtained from later repetitions of the same pattern within the stress step tests, indicating that the time-dependent changes in the data are not substantial. The stress step data show a continuation of the trends established by the ascending stress steps: values of η_{app} increase with σ (Fig. 1(a)). The increase in η_{app} with increasing σ is dramatic because values of $\bar{\dot{\gamma}}_{\text{app}}$ tend to decrease with increasing σ. This is shown by a plot of $\eta_{\text{app}}(\bar{\dot{\gamma}}_{\text{app}})$, in which an increase in η_{app} is associated with a decrease in $\bar{\dot{\gamma}}_{\text{app}}$ (Fig. 1(c)).

During each of the controlled stress experiments, the rheometer provides measurements of the normal force, f, exerted on the parallel plates. For homogeneous flow, f can be related to the difference between the first and second normal stress differences, N_1, and N_2 according to

$$N_1 - N_2 = \left(f/\pi R^2\right)\left(2 + \frac{d \ln f}{d \ln \dot{\gamma}}\right), \tag{1}$$

where R is the radius of the plate. Comparisons between normal force measurements performed on both parallel plate geometries and cone and plate geometries have shown that N_2 is small relative to N_1 (Fall et al. 2008). We therefore report our results in terms of an apparent first normal stress difference $N_1^{\text{app}} = 2f/\pi R^2$, neglecting the second term in Eq. 1 (Larsen et al. 2010; Laun 1994). A similar formula has been used to report normal stresses of dilatant flows in samples that did not exhibit flow homogeneity, causing the formalism relating the local first and second normal stress differences to f to be invalid (Brown and Jaeger 2012).

During the ascending σ tests performed between 0.1 Pa and approximately σ_c, average values of N_1^{app} are provided by the rheometer for each value of σ. For the stress step experiments at higher σ, values of N_1^{app} are calculated for each σ by averaging values of f provided by the raw data tool provided at a rate of 250 points per second.

These measurements reveal that for $\sigma < \sigma_c$, values of N_1^{app} change little with σ. However, as σ approaches σ_c, there is a small decrease in N_1^{app} followed by a significant increase in N_1^{app} as σ ascends further into the solid-like regime. This indicates that the sample is dilatant; the force is caused by the dilation of the particle phase relative to the liquid phase (Cates et al. 2005; Lootens et al. 2005). Conceptually, the dilation can be visualized in terms of layers of closely packed particles parallel to the plates. Particles in a given layer must "roll over" particles in adjacent layers to accommodate shear (Fall et al. 2008). These motions produce networks of particle contacts that span the distance between the plates (Cates et al. 1998). The increase in N_1^{app} with increasing σ implies that larger shear stresses are accommodated by the storage of additional stress in the contacts between particles (see Fig. 1(b)) (Larsen et al. 2010; Brown and Jaeger 2012).

In the solid-like state, irreversible aggregation may disrupt the reproducible state that had been established in the experiments performed immediately after loading. Time-dependent changes also arise from the loss of sample that occurs in some experiments, particularly with samples of spherical particles. To characterize these effects, we conclude each set of experiments by repeating the ascending and descending stress step tests between 0.1 and 45 Pa. Final values of η_{app} are greater than the initial values, but generally not by more than a factor of two. Results obtained using the dumbbell particles are more reproducible than results obtained using spherical particles and exhibited little time dependence.

Flow fluctuations at high temporal resolution

Time-averaged flow curves are useful for establishing the existence of shear thickening and dilatancy; however, they are insufficient for elucidating the mechanisms responsible for the unstable nature of these flows. We further characterize the flow instabilities using the raw data collection tool provided by the manufacturer of the rheometer. These data reveal rapid decreases in $\dot{\gamma}_{\text{app}}$, followed by a gradual return to the steady $\dot{\gamma}_{\text{app}}$ value, as shown for the spherical particles at 59.4 % volume in Fig. 2(a). The first of these events occurs at values of σ that are approximately 10–30 Pa lower than σ_c: 87 Pa for $\varphi = 57.3$ %, 81 Pa for $\varphi = 58.3$ %, and 32 Pa for $\varphi = 59.4$ %.

During rapid changes in $\dot{\gamma}_{\text{app}}$, the stress in the sample, σ_S, can differ from the constant applied stress, σ, because of the inertia of the rheometer. The relationship between these variables is governed by the equation of motion for the rotation of the rheometer:

$$a\ddot{\gamma}_{\text{app}} + \sigma_S = \sigma. \tag{2}$$

In this expression, a is proportional to the rotational inertia, I, of the rheometer:

$$a = I F_\sigma / F_\gamma, \tag{3}$$

where F_σ and F_γ are the standard conversion factors for converting torque and displacement of the rheometer to stress and strain, respectively. Here, we ignore the torque contribution due to friction in the bearing, which is small relative to σ_S.

Using Eq. 2, we calculate σ_S at all times while the system is flowing. This requires a second derivate of the raw displacement data. This is obtained by first using a backward difference derivate to calculate $\dot{\gamma}_{\text{app}}$. We then moderately smooth values of $\dot{\gamma}_{\text{app}}$ using a Savitzky-Golay algorithm, available in MATLAB®, and then perform a second backward difference derivate to obtain $\dot{\gamma}_{\text{app}}$. We validate this approach by using it to analyze raw data obtained from a series of stress step tests performed on calibration oil. For all

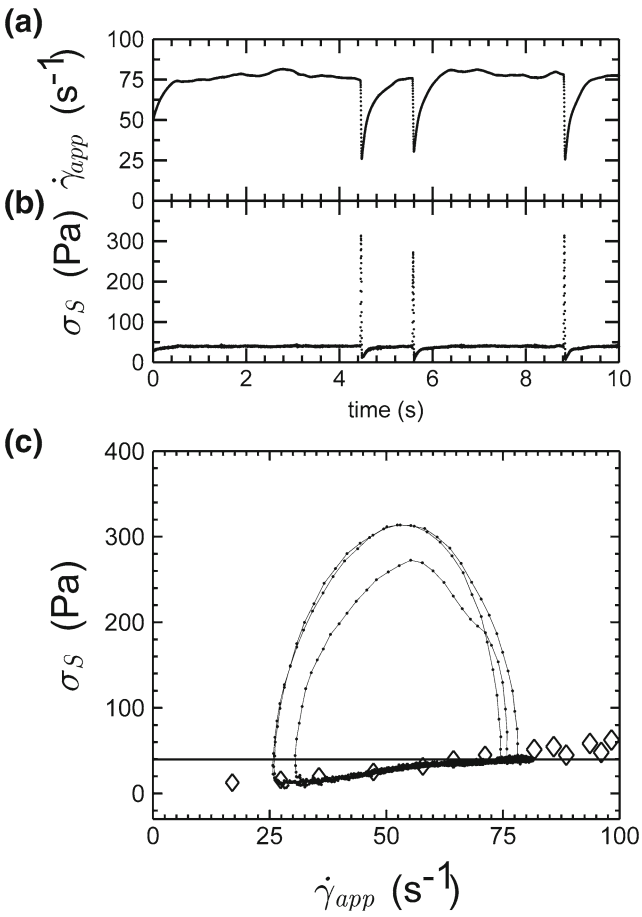

Fig. 2 Time dependence of (**a**) apparent shear rate, $\dot{\gamma}_{\text{app}}$, and (**b**) sample stress, σ_S, during the application of constant stress, σ = 40 Pa, during an ascending stress step experiment on spherical particles at φ = 59.4 %. During each rapid deceleration of the rheometer, the sample adsorbs significant inertial stress from the rotating rheometer. Each time the rheometer subsequently accelerates, it moves along the same line in the space ($\dot{\gamma}_{\text{app}}, \sigma_s$), as shown in (**c**). This near-Newtonian line corresponds to the time-averaged measurements of $\dot{\gamma}_{\text{app}}$ and σ provided by the rheometer in the range of 10 Pa $< \sigma < \sigma_c$, as shown by the *diamond symbols* in (**c**). After acceleration, the rheometer reaches a steady rate of rotation, proportional to $\dot{\gamma}_{\text{app}}$, and the sample stress, σ_S, equals the applied stress, σ = 40 Pa, shown by the *horizontal line* in (**c**)

times, instantaneous values of σ_S are directly proportional to $\dot{\gamma}_{\text{app}} = \dot{\gamma}$, with the constant of proportionality equal to the viscosity of the calibration oil. This confirms that material properties can be accurately measured at millisecond timescales, even during transient periods when σ_S differs substantially from σ (Larsen et al. 2010).

We calculate values of σ_S during the fluctuations in $\dot{\gamma}_{\text{app}}$ which are shown in Fig. 2(a). These calculations show that during a sudden decrease in $\dot{\gamma}_{\text{app}}$, values of σ_S can spike to values that are significantly higher than σ (Fig. 2(b)). High values of σ_S occur because the shear-thickened sample rapidly slows the rotating rheometer, thereby adsorbing significant inertial stress from the rheometer (Nakanishi et al. 2012). Following the rapid deceleration to low $\dot{\gamma}_{\text{app}}$, the sample cannot sustain the applied stress, σ. Therefore, $\sigma_S < \sigma$, and Eq. 2 requires that the rheometer accelerates. As $\dot{\gamma}_{\text{app}}$ increases, σ_S increases as an approximately linear function of $\dot{\gamma}_{\text{app}}$, as shown in Fig. 2(c). As σ_S approaches σ, values of $\dot{\gamma}_{\text{app}}$ recover to a steady state, and no inertial stress is present. The plateau in $\dot{\gamma}_{\text{app}}$ continues until another fluctuation occurs, and the cycle begins again.

The constant proportionality between $\dot{\gamma}_{\text{app}}$ and σ_S during the recovery periods of increasing $\dot{\gamma}_{\text{app}}$ suggests the presence of a near-Newtonian behavior. This "liquid-like" state is reproducible: lines of $\sigma_S(\dot{\gamma}_{\text{app}})$ from each of the recovery periods superimpose onto the same line (Fig. 2(c)). This line also overlaps with averaged values of $\dot{\gamma}_{\text{app}}$ that are obtained from the plateau in η_{app} for 10 Pa $< \sigma < \sigma_c$, as shown by the diamond symbols in Fig. 2(c). Deviations from the near-Newtonian behavior are stochastic in nature; each manifestation of solid-like behavior follows a different trajectory in the $\left(\dot{\gamma}_{\text{app}}, \sigma_S\right)$ space (Fig. 2(c)). Plots of the instantaneous data within the $\left(\dot{\gamma}_{\text{app}}, \sigma_S\right)$ space suggest a simple graphical method for distinguishing liquid-like, or apparent near-Newtonian behavior, from "solid-like" behavior at millisecond timescales. The sample exhibits liquid-like behavior at times that lie along the line of constant proportionality between $\dot{\gamma}_{\text{app}}$ and σ_S, and solid-like behavior at times that lie above this line, during the shear thickening events when $\dot{\gamma}$ decreases rapidly.

The shear thickening events near $\sigma = 40$ Pa are sporadic and can be separated by up to several seconds (see Fig. 2(a)). However, as σ increases further, the large fluctuations occur more often (Fig. 3). The near-Newtonian regime, even at the highest values of $\dot{\gamma}_{\text{app}}$, cannot support the applied stress and σ_S ¡ σ, as shown by the horizontal line in Fig. 3(c). Steady values of $\dot{\gamma}_{\text{app}}$ are not obtained because each period of increasing $\dot{\gamma}_{\text{app}}$ is interrupted by a sudden transition to solid-like behavior that produces a rapid change from acceleration of the rheometer to deceleration. For most of these transitions, the solid-like state vanishes immediately after the low values of $\dot{\gamma}_{\text{app}}$ are obtained. By contrast, occasionally, the solid-like state persists for a fraction of a second at low values of $\dot{\gamma}_{\text{app}}$, where it exhibits smaller fluctuations, as shown in Fig. 3(a, b). In the ($\dot{\gamma}_{\text{app}}, \sigma_S$) plane, these low $\dot{\gamma}_{\text{app}}$ fluctuations produce a series of loops that move in the counterclockwise direction, as shown in Fig. 3(b). As σ increases further, eventually a critical stress is reached at which the low $\dot{\gamma}_{\text{app}}$ fluctuations persist, and there are no recoveries, or few recoveries, to the higher values of $\dot{\gamma}_{\text{app}}$, as shown in Fig. 4. For the spherical particles shown here, the persistent values of low $\dot{\gamma}_{\text{app}}$ are first observed at $\sigma = 180$ Pa for $\varphi = 59.4$ %, and at $\sigma = 400$ Pa for $\varphi = 58.3$ % and $\varphi = 57.3$ %. The persistent values of low $\dot{\gamma}_{\text{app}}$ are similar to the minimum values of $\dot{\gamma}_{\text{app}}$ observed during the brief moments of solid-like behavior. The transition to the

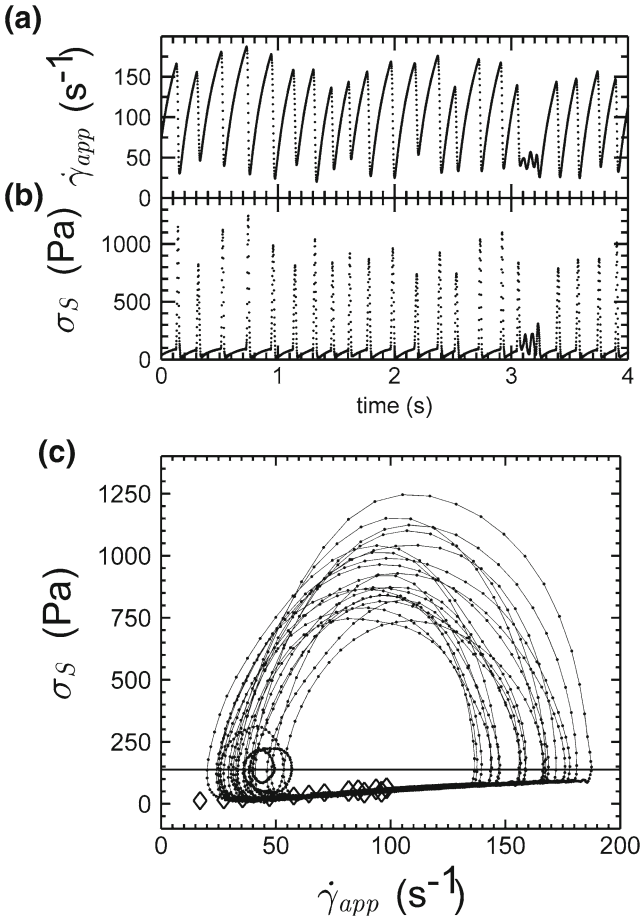

Fig. 3 Time dependence of (**a**) apparent shear rate, $\dot{\gamma}_{\text{app}}$, and (**b**) sample stress, σ_S, during the application of constant stress, σ = 140 Pa, during an ascending stress step experiment on spherical particles at φ = 59.4 %. During each rapid deceleration of the rheometer, the sample adsorbs significant inertial stress from the rotating rheometer. Each time the rheometer subsequently accelerates, it moves along the same line in the space ($\dot{\gamma}_{\text{app}}, \sigma_s$), as shown in (**c**). This near-Newtonian line corresponds to the time-averaged measurements of $\dot{\gamma}_{\text{app}}$ and σ provided by the rheometer in the range of 10 Pa $< \sigma < \sigma_c$, as shown by the *diamond symbols*. Following acceleration, the rheometer does not reach a steady rate of rotation. Values of σ_S remain below the applied stress, σ = 140 Pa, shown by the *horizontal line* in (**c**), until another rapid deceleration occurs, thereby starting the cycle again

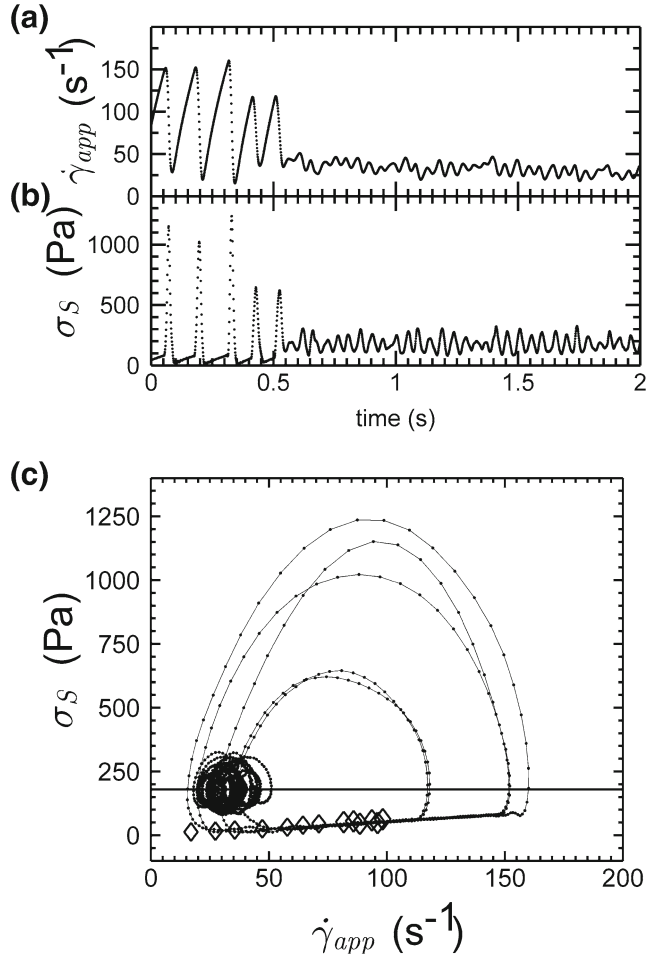

Fig. 4 Time dependence of (**a**) apparent shear rate, $\dot{\gamma}_{\text{app}}$, and (**b**) sample stress, σ_S, during the application of constant stress, σ = 180 Pa, during an ascending stress step experiment on spherical particles at φ = 59.4 %. During each of the five rapid deceleration events shown, the sample adsorbs significant inertial stress from the rotating rheometer. Each time the rheometer subsequently accelerates, it moves along the same line in the space ($\dot{\gamma}_{\text{app}}, \sigma_s$), as shown in (**c**). This line corresponds to the time-averaged measurements of $\dot{\gamma}_{\text{app}}$ and σ provided by the rheometer in the range of 10 Pa $< \sigma < \sigma_c$, as shown by the *diamond symbols*. Following acceleration, the rheometer does not reach a steady rate of rotation. Values of σ_S remain below the applied stress, σ = 180 Pa, shown by the *horizontal line* in (**c**), until another rapid deceleration occurs, thereby starting the cycle again. The large fluctuations persist for approximately the first 0.5 s of the σ step, after which the sample transitions to a persistent state of dilatancy, characterized by smaller fluctuations

persistent values of low $\dot{\gamma}_{\text{app}}$ corresponds to a significant increase in the value of N_1^{app} that is measured by the rheometer (Fig. 1(a)). We therefore associate the low $\dot{\gamma}_{\text{app}}$ values with the dilatant regime. For this reason, we conclude that the temporary periods of solid-like behavior observed during the fluctuations are transient manifestations of dilatancy.

Slip analysis

To investigate the extent to which spatial heterogeneities may be responsible for the observed temporal fluctuations, we measure the flow curves of one of our samples (spherical particles at $\varphi = 58.3$ %) at gap heights, d, of 1250, 950, 750, and 550 ∝m. In the gradual shear thickening regime for $\sigma < 10$ Pa, values of η_{app} are consistent for all gap heights, as shown in Fig. 5(a). At higher σ, samples at all d exhibit a plateau in η_{app}. In this region, the plateau values of η_{app} increase with increasing d. This indicates that the assumption of homogeneous flow in the gap is violated in this portion of the flow curve.

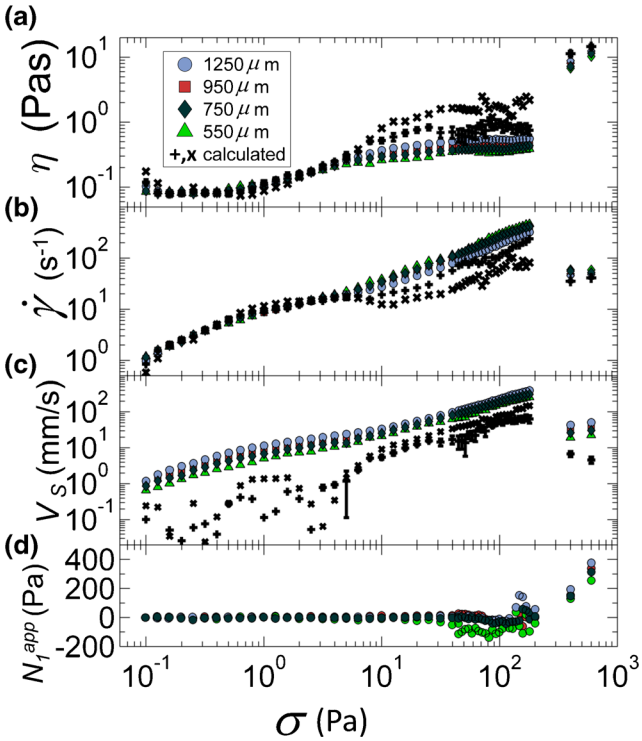

Fig. 5 Gap-dependence of (**a**) viscosity, (**b**) shear rate, and (**c**) slip velocity for spherical particles, φ = 58.3 %. Values of the apparent viscosity, η_{app}, apparent shear rate, $\dot{\gamma}_{\text{app}}$, and linear velocity, V, of the outer rim of the upper plate are shown by the *closed symbols*. Values of the true viscosity, η, true shear rate, γ, and the slip velocity, V_S, are shown by the $+$*symbols* (calculated from all four gap heights) and $\times$*symbols* (calculated for two largest gap heights). The uncertainty bars on the $+$ *symbols* are only shown for $\sigma > 3$ Pa, where the slip becomes sufficiently large to be quantified. (**d**) The apparent first normal stress difference, N_1^{app}, shows little dependence on the gap height. The onset of dilatancy corresponds to a significant decrease in both V_S and V

Similar gap dependence in extremely shear thickening materials has been attributed to apparent wall slip or wall slip (Laun et al. 1991; Lee and Wagner 2003; Yilmazer and Kalyon 1991). Direct visualization of shear thickening materials in a Couette cell has revealed a stationary plug that nearly fills the gap, with apparent wall slip on both walls (Boersma et al. 1991). Wall slip in suspensions of hard particles may be caused by geometrical packing effects that cause the density of particles near the wall to be lower than in the bulk (Laun and Hirsch 1989; Kalyon 2005). This causes the shear rate in the region that is adjacent to the wall to be greater than the shear rate of the bulk.

In general, wall slip is more likely to occur when smooth geometries are used (Barnes 1995). Additional measurements performed using smooth parallel plates with similar particles also exhibited qualitatively similar flow curves, including the plateau in η_{app} where the flow inhomogeneity occurs. It is likely that this plateau is caused by wall slip, and that the roughness of the plates that we use in experiments reported here is insufficient to prevent wall slip from occurring. Moreover, our system is not density-matched, and even a small amount of sedimentation will exacerbate particle depletion at the upper plate. Observations of identical flow curves for both smooth and roughened plates have been reported in shear thickening suspensions that exhibit sedimentation (Brown and Jaeger 2012). The behavior is attributed to the presence of a fluid-filled gap between the upper layer of particles and the upper plate. Velocimetry measurements obtained with video microscopy on these systems reveal that because of this gap, the velocity of the upper layer of particles is less than the velocity of the upper plate. Dilation of the particle phase causes particles in the upper layer to penetrate into the gap. The dilation therefore decreases the local volume fraction in the particle phase and causes it to become fluidized, thereby forming a shear band. The width of the shear band increases as σ increases from rest.

Our system differs from these systems because it exhibits homogeneous, or gap-independent, shear thickening at low stress ($<$ 10 Pa) before transitioning to a inhomogeneous regime at higher stress ($>$ 10 Pa). Inhomogeneous flow may emerge in our system due to the formation of shear-induced aggregates. The aggregates resist shear and form a solid-like "plug" region in the bulk of sample, while shear bands or slip layers form close to the walls. Aggregated particle clusters may also sediment, allowing the formation of a gap between the upper layer of particles and the upper plate.

Because it is likely that wall slip occurs in our system, we characterize the measured gap dependence of our measurements using a standard wall slip analysis. Wall slip is modeled with the following equation:

$$\dot{\gamma}_{\text{app}} = \dot{\gamma} + 2\frac{V_{\text{s}}}{d} \tag{4}$$

where $\dot{\gamma}_{\text{app}}$ is the apparent shear rate, $\dot{\gamma}$ is the true, or bulk, shear rate, and V_s is the slip velocity, or the difference in the velocity of the outer rim of the plate, and the portion of the sample that is adjacent to it, and only separated from it by a thin region that is solvent-rich (Yoshimura and Prudhomme 1988; Yoshimura et al. 1987). We assume that V_s and $\dot{\gamma}$ depend only on σ and are independent of d, and we use Eq. 4 to estimate V_s and $\dot{\gamma}$ at each value of σ by performing a least-squares linear fit to the data points at coordinates $(2/d, \dot{\gamma}_{\text{app}})$.

This method requires that for a given gap height, a representative value of $\dot{\gamma}_{\text{app}}$ be chosen for each value of σ. For low σ, we use the steady-state value of $\dot{\gamma}_{\text{app}}$, obtained by averaging over the final seconds of the time that a given σ was applied. However, for $\sigma > \approx 80$ Pa, large fluctuations are present, and the rheometer does not reach a steady state

(Figs. 3(c) and 4(c)). It is therefore not immediately obvious how to select a representative value of $\dot{\gamma}_{\text{app}}$ for a given σ. One option is to select an average value of $\dot{\gamma}_{\text{app}}$ over the time period that σ is applied. However, average values of $\dot{\gamma}_{\text{app}}$ depend on both the dilatant state and apparent near-Newtonian state, and their relative frequency of appearance. To facilitate a clear interpretation of our slip analysis, we applied the analysis only to the portion of the data that pertains to the apparent near-Newtonian state, or liquid-like state.

This requires that a single representative value of $\dot{\gamma}_{\text{app}}$ for each value of σ be calculated from pairs of $(\dot{\gamma}_{\text{app}}, \sigma_S)$ data points obtained from the raw data collected at 4-ms time intervals over the entire step of constant σ. We do this calculation for a given value of σ and d by first binning the data pairs $(\dot{\gamma}_{\text{app}}, \sigma_S)$ from each time point of 4 ms into an array of bins, linearly distributed in $\dot{\gamma}_{\text{app}}$. For each bin of $\dot{\gamma}_{\text{app}}$, we find the minimum value of σ_s from all the data pairs $(\dot{\gamma}_{\text{app}}, \sigma_S)$ that fall into that bin. This approach assures that points in the liquid-like regime are selected rather than the points in the solid-like, or dilatant, regime. These values of σ_S, together with the middle values of $\dot{\gamma}_{\text{app}}$ from each bin, define an approximately straight line in $(\dot{\gamma}_{\text{app}}, \sigma_S)$ space, corresponding to the apparent near-Newtonian state. A linear fit to these points defines A and B in the relationship, $\sigma_s = A\dot{\gamma}_{\text{app}} + B$. Values of A and B are then used to calculate a representative value of $\dot{\gamma}_{\text{app}}$ for the particular value of σ that is applied. This calculation is performed for each of the values of σ used in the ascending stress steps, $\sigma <$ 180 Pa. Because only data in the near-Newtonian regime is used for this calculation, an increase in $\eta_{\text{app}} = \sigma/\dot{\gamma}_{\text{app}}$ at σ_C is not apparent in Fig. 5(a).

From values of $\dot{\gamma}_{\text{app}}$ calculated from all four values of d, we use Eq. 4 to calculate V_S and $\dot{\gamma}$. Values of $\dot{\gamma}$ are then used to calculate a true viscosity, $\eta = \sigma/\dot{\gamma}$, at each value of σ. These values of η pertain only to the liquid-like or apparent near-Newtonian regime and not to the dilatant regime. To our knowledge, this is the first time that a slip correction has been calculated for a state that appears only transiently, during a fluctuation.

Calculated values of η and $\dot{\gamma}$ are consistent with values of η_{app} and $\dot{\gamma}_{\text{app}}$ measured during gradual shear thickening for σ <10 Pa (Fig. 5(a, b)). This is consistent with the fact that values of η_{app} and $\dot{\gamma}_{\text{app}}$ in this regime are independent of d. However, as the material enters the regime in which values of η_{app} plateau for all gap heights d, the calculated values of η continue to increase with σ (+ symbols in Fig. 5(a)). The slope of this increase is approximately consistent with the slope $d\eta/d\sigma$ in the continuous shear thickening regime (Fig. 5(a)). This corresponds to a gradual increase in $\dot{\gamma}$ with increasing σ in the apparent near-Newtonian regime (+ symbols in Fig. 5(b)). For $\sigma > 20$ Pa, values of η begin to plateau. As this occurs, the uncertainty associated with

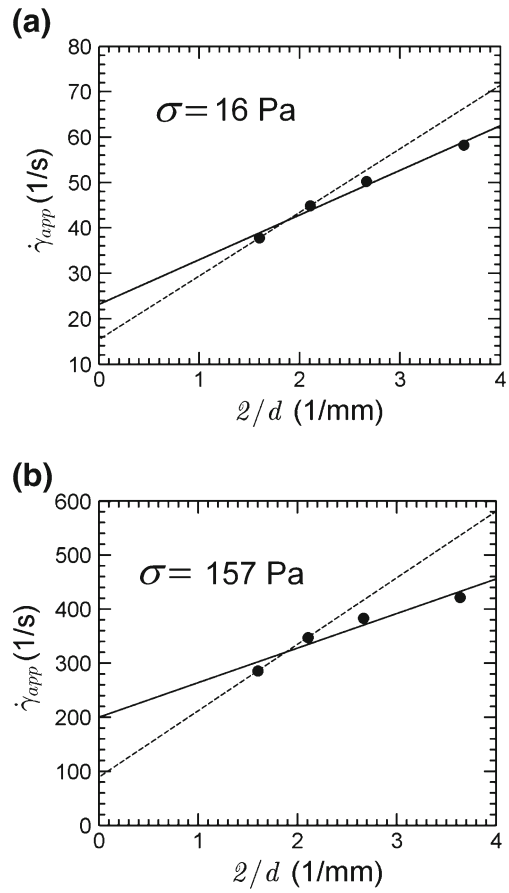

Fig. 6 Linear fits to $\dot{\gamma}_{\text{app}}$ as a function of $2/d$ are used to calculate slip properties using Eq. 4. Each *circle symbol* denotes representative values of $\dot{\gamma}_{\text{app}}$ obtained from the raw data as described in the text; the uncertainty of these measurements is small relative to the symbol size. The $\dot{\gamma}_{\text{app}}$ intercept at $2/d = 0$ is taken to be the true shear rate, $\dot{\gamma}$, and the slope of the fit is taken to be the slip velocity, V_S. Fits obtained using all four values of d are shown by the *solid lines*. However, this approach is only an approximate representation of the data, which exhibit negative curvature, or a decrease in V_S with decreasing d. At low σ, the deviation from linearity is not severe as shown in (**a**) for σ = 16 Pa. However as σ increases, the curvature because more pronounced as shown in (**b**) for σ = 157 Pa. When this occurs, values of $\dot{\gamma}$ can be more accurately estimated using data from only the two largest values of d. These fits are shown with the *dashed lines*

the linear fit to the data points at coordinates ($2/d$, $\dot{\gamma}_{\text{app}}$) increases, as shown in Fig. 5(a). This increase in uncertainty is due to the negative or downward curvature in these points, as shown in Fig. 6. This negative curvature is consistently observed in the range of 10 Pa $< \sigma <$180 Pa. Within the simple model of slip, the slope of $\dot{\gamma}_{\text{app}}$ as a function of $2/d$ is a measure of the slip velocity, V_S. The negative curvature in the $(2/d, \dot{\gamma}_{\text{app}})$ space therefore corresponds to a decrease in V_S as the gap height, d, decreases. In this case, $\dot{\gamma}$ is still defined as the limiting value of $\dot{\gamma}_{\text{app}}$ as $2/d$ approaches zero. This limit is best determined by evaluating data only at largest values of d. We therefore perform

a second calculation of $\dot{\gamma}$ and V_S by only using the data at the largest gap heights, 1250 and 950 ∝m. This approach gives rise to values of $\dot{\gamma}$ that are lower, and values of V_S that are larger than those calculated using data from all four gap heights (see × symbols in Fig. 5). Values of η calculated with this approach continue to increase until approximately $\sigma = 40$ Pa, when there is another plateau in η. We hypothesize that, as with the plateau observed when all four values of d were used to calculate η, this plateau is also an artifact that is caused by curvature of $\dot{\gamma}_{\text{app}}$ with respect to $2/d$ and would not be present if we had more data available at even larger values of d, where the limiting behavior as $2/d$ approaches zero can be assessed more accurately. We therefore expect that in this plateau region, as σ approaches the dilatant regime, our calculations using two values of d underestimate the true values of both V_S and η. We also expect that the use of the two largest values of d gives more accurate estimates of $\dot{\gamma}$ than the use of four values of d, and we use the former approach for all subsequent calculations in the liquid-like regime, where σ <180 Pa. Nevertheless, regardless of the approach used, our measurements clearly indicate that substantial flow inhomogeneity, most likely slip or shear banding, is present in the apparent Newtonian plateau between the gradual shear thickening regime and the dilatant regime. We therefore refer to this regime as the apparent wall slip regime, or the slip-dominated regime.

To characterize slip in the dilatant regime, we perform the same analysis on the data obtained by the stress step tests at $\sigma = 400$ and 600 Pa. This is done by using Eq. 4, but with $\dot{\gamma}_{\text{app}}$ replaced by a mean apparent shear rate, $\bar{\dot{\gamma}}_{\text{app}}$, obtained by averaging $\dot{\gamma}_{\text{app}}$ over all times that a given σ is applied. We also replace $\dot{\gamma}$ in Eq. 2 with an average true shear rate, $\bar{\dot{\gamma}}$. Calculated values of $\eta = \sigma/\bar{\dot{\gamma}}$ in the dilatant regime, 400 and 600 Pa, using all four values of d, are shown by the black "+" symbols in Fig. 5(a).

As the material enters the dilatant regime, values of V_S exhibit a dramatic decrease from 150 mm/s at 180 Pa to 7 mm/s at 400 Pa (Fig. 5(c)). Moreover, the relative contribution of slip to the total rotation also decreases. In the apparent wall slip regime, 120 Pa $< \sigma <$ 180 Pa, the average ratio of V_S to the linear velocity, $V = \dot{\gamma}_{\text{app}} d$, of the outer rim of the upper plate is 0.37 for $d = 950$ ∝m. However, in the dilatant regime at $\sigma = 400$ and 600 Pa, the average value of V_S/V is 0.16 at $d = 950$ ∝m.

Within the dilatant regime, V_S decreases from 7 ± 1 to 5 ± 1 mm/s as σ increases from 400 to 600 Pa. This corresponds to an increase in $\dot{\gamma}$ from 35 ± 3 to 41 ± 2 s^{-1} even as $\dot{\gamma}_{\text{app}}$ remains independent of σ. This is consistent with observations from NMR (Fall et al. 2010) and video microscopy measurements (Brown and Jaeger 2012; Boersma et al. 1991) showing that even when a bulk flow curve is discontinuous, the local stress/strain relationships at locations spanning the gap are not discontinuous.

The significant reduction in slip associated with the transition to dilatancy corresponds to an increase in values of N_1^{app} for all gap heights (Fig. 5(d)). Values of N_1^{app} do not depend significantly on the gap height and are proportional to σ (Larsen et al. 2010). We calculate the constant of proportionality, c, in the relation $N_1^{\text{app}} = c\sigma$ with a linear fit to average values of N_1^{app} at 200, 400, and 600 Pa. Values of c do not vary greatly with the gap height and are 0.8 for d = 1,250, 950, and 750 ∝m, and 0.7 for d = 550 ∝m.

The observed curvature of $\dot{\gamma}_{\text{app}}$ as a function of $2/d$ in the range of 10 Pa $< \sigma <$180 Pa suggests that V_S is not independent of d, as is usually assumed, but that it decreases as d decreases. If samples at lower d exhibit less wall slip, and if the onset of dilatancy requires that the frictional stresses associated with dilatancy arrest, or diminish, wall slip, then it is reasonable to expect that the onset of dilatancy will occur at lower σ for lower gap heights. To test this hypothesis, we observe that for d=1250, 950, 750, and 550 ∝m, intermittent dilatancy first occurs at 71, 81, 67, and 34 Pa, respectively. The lowest σ for the onset of dilatancy is therefore observed at the smallest gap height, which is consistent with previous findings (Chow and Zukoski 1995; Fall et al. 2008). These results imply that as the gap height decreases, samples are more likely to exhibit dilatancy and less likely to exhibit wall slip.

Discussion

Our observations show that the apparent wall slip depends on σ. For 1 Pa $< \sigma <$10 Pa, wall slip is not significant, and the flow profile is homogeneous within the shear thickening regime. However, the increase in η_{app} with σ is interrupted by the onset of significant apparent wall slip near 10 Pa. Our slip analysis suggests that the apparent wall slip "hides" a continued increase in η within the bulk liquid; this result is consistent with previous observations (Yilmazer and Kalyon 1991). These authors also showed that as σ increases within the shear thickening regime, and the slip velocity also increases until virtually all of the rotation is attributed to wall slip. Our material exhibits a similar effect; however, this effect is interrupted when the dilatant state emerges, decreasing the slip velocity and the relative contribution of the apparent slip to the total rotation of the upper plate.

The transition from the slip-dominated regime to the dilatant regime is marked by a series of rapid fluctuations between the two states. To develop models of the large fluctuations, it may first be necessary to understand the mechanism by which dilatancy reduces wall slip. In general, wall slip occurs when there is a lack of adhesion between the particle clusters and the wall (Barnes 1995). At the onset

of dilatancy, the outmost particles of the clusters are pushed away from the sample center and forced into contact with the wall, thereby increasing the friction between the particles and the wall and dramatically reducing the wall slip. As σ is increased within the dilatant regime, increased friction between the particles and the wall causes N_1^{app} to increase, leading to a further reduction in V_S.

These results therefore suggest that there is a competition between the slip and the dilatancy that is analogous to the well-known model of the relationship between friction and the normal force. In this model, the tangential friction force between an object and a planar surface is proportional to the normal force between the object and the plane. The normal force provides an effective adhesion between the object and the planar surface by allowing the development of frictional forces that prevent the object from sliding when a tangential force is applied. Similarly, the normal force of the dilatant sample increases the friction between the sample and the roughened plates, thereby reducing apparent wall slip, or the "sliding" of the sample relative to the wall.

The transition from the slip regime to the dilatant regime depends on the applied stress: at low stress, the slip regime dominates, and at high stress, the dilatant regime dominates. However, there is a wide range of intermediate stresses at which the neither regime is dominant, and the system exhibits intermittent and semi-regular oscillations between the slip regime and the dilatant regime. From the instantaneous measurements of sample stress, σ_S, shown in Figs. 2, 3, and 4, it is apparent that for a given value of instantaneous stress, the material can exist in either the slip regime or the dilatant regime, but it cannot exist in either regime in a stable manner. The particular state that the system exhibits at a given moment is sensitive to $\dot{\gamma}_{\text{app}}$. Systems at high $\dot{\gamma}_{\text{app}}$ transition to the dilatant state, and systems at low $\dot{\gamma}_{\text{app}}$ transition to a state dominated by apparent wall slip. The dilatant state requires a large $\dot{\gamma}_{\text{app}}$ to be triggered, but it cannot be sustained at the low values of $\dot{\gamma}_{\text{app}}$ that result from the triggering of the dilatant state. Therefore, at low $\dot{\gamma}_{\text{app}}$, dilatancy vanishes. Because the low value of $\dot{\gamma}_{\text{app}}$ is insufficient to support the applied stress within the apparent wall slip regime, the rheometer accelerates until a sufficiently high value of $\dot{\gamma}_{\text{app}}$ is reached to trigger dilatancy again.

A better understand of this instability clearly requires an understanding of the role played by $\dot{\gamma}_{\text{app}}$ in driving dilatancy. Our slip analysis shows that within the apparent wall slip regime, an increase in σ, or $\dot{\gamma}_{\text{app}}$, maybe is associated with a gradual increase in γ (Fig. 5(b)). The shear rate of a granular system plays a critical role in determining the particle pressure or the pressure that characterizes the tendency of a sheared particle phase to expand relative to the solvent phase. This expansion pressure is balanced by a suction pressure in the solvent (Deboeuf et al. 2009). This pressure is measured in an experiment in which the solvent of a sheared suspension is connected to a liquid reservoir from which the particles are excluded by a fine mesh (Deboeuf et al. 2009). During shear, the expansion of the dense non-Brownian particle phase produces a negative liquid pressure that tends to drain the reservoir. This pressure increases linearly with the shear rate of the particle phase.

Within the apparent wall slip regime, the slip region, or the shear band region, near the upper plate may be water-rich relative to the bulk material, due to particle exclusion effects near the boundary (Laun and Hirsch 1989; Kalyon 2005) or particle sedimentation. The water-rich region may therefore be susceptible to being drained by the particle-rich portion of the sample when the particle-rich, or bulk, region is sheared at a sufficiently high rate. At moderately high values of $\dot{\gamma}_{\text{app}}$, or $\dot{\gamma}$, dilation imparts fluidity to the particle-rich portion of the sample because of a decrease in volume fraction caused by the suction of liquid from the water-rich region into the bulk phase. If the rheometer accelerates to higher $\dot{\gamma}_{\text{app}}$, the water in the "water-rich" region will be sufficiently depleted that the outermost particles of the bulk phase will form frictional contacts with the wall. Frictional stresses will be transmitted between the plates via particle plate contacts and via networks of particle-particle contacts. At this moment, the dilatation switches from being a mechanism to promote particle fluidity to becoming a mechanism to support extended networks of frictional contacts. Because of the solid-like nature of the frictional contacts, the flow in the particle phase decreases to a lower-average shear rate. The decrease in the shear rate gives rise to a decrease in particle pressure. The decrease in the particle pressure leads to a reduction of the tendency of the particle phase to expand outwards. This leads to a lower "adhesion" of the outer particle layer to the plate thereby permitting the solvent-rich slip or shear band layer to reform. The material returns to the apparent wall slip regime, which cannot support the applied stresses at the low shear rate prescribed by dilatancy. The rheometer therefore accelerates, and the cycle begins again.

Within this cycle, dilatancy plays two roles. It is a mechanism that promotes the fluidity of the particle phase by allowing the bulk phase to adsorb nearby water, and it is a mechanism to support extended networks of frictional contacts between particles. The first mechanism requires high shear rates, and the second mechanism prescribes much lower shear rates. If this is true, then fluctuations during dilation may be a manifestation of the dual and contradictory functions that dilatation plays: although dilation can fluidize dense suspensions, it may also lead to arrested fluidity when rigid boundaries are encountered. This dual nature of dilatancy is born out by experiments showing that in the

absence of a confining boundary, dilatancy can fluidize suspensions; however, when the dilatating particles encounter a confining boundary, the result is a dramatic loss of fluidity or shear thickening (Brown and Jaeger 2012; Fall et al. 2008).

For sufficiently high values of σ, the dilatant state is not a transient manifestation, but rather is able to persist, even at the low values of $\dot{\gamma}_{\mathrm{app}}$. If the particle pressure is an increasing function of the true shear rate, $\dot{\gamma}$, then we would expect the particle pressure to increase with σ and $\dot{\gamma}$ within the dilatant regime. This is consistent with the observed increase in N_1^{app} and $\dot{\gamma}$ as σ increases from 400 to 600 Pa in the dilatant regime. Within the persistent dilatant regime, both fluctuations and apparent wall slip are present; we therefore expect that the mechanisms that cause the largest fluctuations at the onset of dilatancy are also present within the persistent dilatant regime.

It is also important to consider additional mechanisms for the observed fluctuations. Our data demonstrate that the appearance of solid-like behavior triggers behavior that is less solid-like. This type of behavior can be interpreted as an apparent yielding of the solid-like state that occurs during dilatancy. Such "yielding" effects have been studied at high stresses at which the macroscopic flow curve transitions from discontinuous shear thickening to shear thinning. This can occur because of the existence of a maximum in the stress that can be carried by the liquid surface against the expanding particle phase. This maximum stress is given by Σ/σ, where Σ is the surface tension of the liquid (O'Brien and Mackay 2000; Cates et al. 2005; Brown and Jaeger 2012). For our system, $\Sigma/\sigma \approx 10^4$ Pa, more than an order of magnitude greater than the maximum σ applied. A second possible source of apparent yielding is the deformation of the particles, which can also give rise to shear thinning (Meeker et al. 2004). The viscosity in this regime is given by $\eta \sim \dot{\gamma}^{-1/2}(\eta_s G)^{1/2}$, where η_s is the viscosity of the solvent, and G is the particle shear modulus (Kalman et al. 2008). Taking G to be the bulk modulus of polystyrene, G= 3 GPa, we calculate that for $\dot{\gamma} = 10$ and 100 s^{-1}, $\eta \approx 600$ and 200 Pa. These values of η are significantly greater than those observed in our measurements and would require values of σ significantly greater than those applied. We therefore conclude that neither surface tension effects nor particle deformation is likely to play a role in producing the observed fluctuations. These effects become significant at higher stresses where discontinuous shear thickening is expected to give way to shear thinning; they are not likely to be significant at the onset of dilatancy where we observe the largest fluctuations.

We also consider the possibility that during the transient manifestations of dilatancy that punctuate the slip-dominated regime, the sample becomes a jammed solid. From visual inspection of Figs. 2(c), 3(c), and 4(c), it is apparent that a single "transient manifestation of dilatancy" lasts for approximately 25 data points, or 100 ms. An average value of the $\dot{\gamma}_{\mathrm{app}}$ over this time is approximately 100 s^{-1}. Our slip estimate predicts that in the dilatant regime, $\dot{\gamma}/\dot{\gamma}_{\mathrm{app}} \approx 0.7$. Therefore, we expect that during a transient manifestation of dilatancy, the apparent strain is approximately 7. A jammed solid would be unlikely to sustain this amount of deformation. We therefore expect that the deformation is taking place within the bulk material during the isolated manifestations of dilatancy and that the material does not behave as a jammed solid.

Extreme shear thickening behavior has also been attributed to a transition from a viscous to an inertial scaling, $\eta \propto \dot{\gamma}$ (Fall et al. 2010). To test whether our material exhibits inertial scaling within the dilatant regime, we calculate n within the relation $\eta \propto \bar{\dot{\gamma}}^n$ for $\sigma = 400$ and 600Pa. We find $n = 1.6$, which is more consistent with inertial scaling than viscous scaling, $n = 0$. Within the inertial regime, particle migration, driven by gradients in the particle pressure, becomes significant (Fall et al. 2010). The rearrangement of the particles causes the disappearance of the transient state of extreme shear thickening behavior. Similarly, our observations suggest that a transient dilatant state gives rise to self-filtration of the particle phase, resulting in dramatic fluctuations during flow.

Because fluctuations are rapid, the inertia of the rheometer can play a role in determining the timescales of the fluctuations. This timescale can provide a measure of an apparent nonlinear elasticity that increases with φ (Larsen et al. 2010). The measurements are likely to be most appropriate at high φ and high σ where the sample exhibits behavior that is more solid-like and less apparent wall slip is present. For lower φ and lower σ, an accurate model of the material response requires a more complete description of the flow inhomogeneity, particularly the interplay between dilatancy and apparent wall slip.

Our observations of fluctuations between a liquid-like state, characterized by continuous shear thickening, and a solid-like state, characterized by frictional contacts, may be related to observations that shear thickening can function as a reentrant glass transition induced by shear stress (Cates et al. 2005). A model of this behavior based on mode coupling theory (MCT) predicts the existence of both a high-viscosity state and low-viscosity state for a given shear rate. These states may coexist during shear banding or may even be present at zero shear rate, accounting for the

bistable nature of stationary granules or droplets of dilatant materials. However, because these states are stable, additional physics are required in the model to account for the observed fluctuations between the states.

Flow fluctuations, both regular and erratic, have also been observed in other complex materials, including surfactant solutions containing worm-like micellar phases (Fischer et al. 2002) or lamellar phases (Salmon et al. 2002). Direct measurements of flow profiles has established that the flow fluctuations result from fluctuating shear bands (Aradian and Cates 2006). In these materials, coexisting flow phases, or textures, are formed that each exhibit distinct rheological properties. Time-dependent changes in the bulk rheological response occur as one region grows at the expense of a neighboring region.

These fluctuations are modeled by incorporating slow structural relaxation into models that describe shear banding (Aradian and Cates 2006; Fielding and Olmsted 2004). These models can reproduce the wide range of flow conditions that are observed experimentally, including regular oscillations and erratic fluctuations. Because both regular and erratic fluctuations occur in dilatant materials, these models may be relevant for describing fluctuations in dilatant materials (Aradian and Cates 2006). Nevertheless, there is a significant difference in the timescales of the fluctuations in surfactant solutions and dilatant suspensions. Fluctuations in surfactant solutions typically occur over timescales of several minutes, which are set by structural relaxation (Salmon et al. 2002). Fluctuations in dilatant suspensions typically occur over 10–100 ms. This timescale is sufficiently rapid that in stress-controlled experiments, it is not independent of the inertia of the rheometer and is therefore not governed only by the properties of the material (Larsen et al. 2010). Despite this difference, we believe that the present work tends to strengthen the likelihood that flow fluctuations in the two classes of materials are related, because our results demonstrate a close relationship between flow inhomogeneities and fluctuations in dilatant materials.

Given the central role of flow inhomogeneities in driving fluctuations in a wide variety of systems, the multiple reports of flow inhomogeneities in dilatant materials, and the central role that flow inhomogeneities play in the fluctuations studied in our system, it is tempting to speculate that flow inhomogeneities may play a role in driving instabilities generally in dilatant materials. If this is true, then we expect that a hydrodynamical model that is able to account for the intermittent slip and dilatant behavior that we observe can perhaps be extended to a general model of flow instabilities in dilatant materials. A model with a phenomenological state variable has been used to predict several of the behaviors exhibited by our materials, including regular oscillations and rapid hardening (Nakanishi et al. 2012). Additional research is needed to determine whether hydrodynamic models of unstable flow in dilatant particle suspensions can be applied to the behavior described here (Mills and Snabre 2009).

Conclusions

Our suspensions exhibit a stress-induced transition from a slip-dominated regime to a dilatancy-dominated regime. However, this transition does not occur at a single critical stress. Rather, there is a range of applied stresses over which the sample exhibits dramatic oscillations between the slip and dilatant regimes because neither regime is capable of supporting stress in a steady manner. For stresses within this intermediate range, the critical determinant of whether the material is entering the slip or dilatant regime is the apparent shear rate, $\dot{\gamma}_{\mathrm{app}}$. Higher values of $\dot{\gamma}_{\mathrm{app}}$ may give rise to greater particle pressure in the particle-rich phase, thereby depleting the slip layer of solvent and triggering a dilatant state. However, the dilatant state is present only long enough to cause a dramatic decrease in $\dot{\gamma}_{\mathrm{app}}$; this is immediately followed by a return to the slip regime. The disappearance of dilatancy may be caused by the fact that at the lower values of $\dot{\gamma}_{\mathrm{app}}$, the particle pressure is too small to prevent the solvent-rich slip layer from reforming. After the sample returns to the slip regime, the rheometer accelerates to higher values of $\dot{\gamma}_{\mathrm{app}}$ where the transient dilatancy is triggered again.

This oscillatory behavior is only observed at stresses that are intermediate between the slip regime and the dilatant regime. As the stress increases from this range into the dilatant regime, particles have a greater tendency to spread outwards, as indicated by the larger values of N_1^{app}. At sufficiently high stresses, the drop in $\dot{\gamma}_{\mathrm{app}}$ persists without a return of the slip-dominated regime. At these stresses, the particle pressure is sufficiently large to produce an effective adhesion of the bulk to the upper plate, thereby preventing the slip-dominated regime from returning. Nevertheless, flow in the dilatant state continues to exhibit both fluctuations and slip.

The interplay play between dilatancy and slip in producing flow fluctuations implies that the fluctuations can arise from the existence of an unstable boundary between the particle-rich region and the solvent-rich region, or slip layer. For a given applied stress, the sample fails to maintain a steady value of the thickness of the slip layer and

therefore cannot maintain a steady value of $\dot{\gamma}_{\mathrm{app}}$. We speculate that this finding may be generalized to other dilatant flows, even in regimes in which slip does not dominate; flow fluctuations in dilatant materials may arise from unstable boundaries between regions of different local volume fractions, different local shear rates, or different local particle pressures. If the boundaries between such regions are unstable, then the various regions may expand and contract as solvent flows from regions of low particle pressure to regions of high particle pressure. The redistribution of solvent will change local values of φ, shear rate, and particle pressure, and thereby alter the direction of solvent transport. A given region could therefore alternate between states of low shear rate and high shear rate as it exchanges solvent with neighboring regions in a stochastic fashion. The resulting macroscopic flow arises from the combined contributions of all the regions and would therefore be expected to exhibit fluctuations that are representative of dilatant materials.

Acknowledgments This work was supported by the NSF (DMR-1006546), the Harvard MRSEC (DMR-0820484), and by the U.S. Department of Energy under Award No. DEFG02-91-ER45439, through the Frederick Seitz Materials Research Laboratory at the University of Illinois at Urbana-Champaign.

References

Aradian A, Cates ME (2006) Minimal model for chaotic shear banding in shear thickening fluids. Phys Rev E 73:041508

Barnes HA (1989) Shear-Thickening (Dilatancy) in suspensions of nonaggregating solid particles dispersed in Newtonian liquids. J Rheol 33:329–366

Barnes HA (1995) A review of the slip (wall depletion) of polymer-solutions, emulsions, and particle suspensions in viscometers—its cause, character, and cure. J Non-Newton Fluid 56:221–251

Bender JW, Wagner NJ (1995) Optical measurement of the contributions of colloidal forces to the rheology of concentrated suspensions. J Colloid Interf Sci 172:171–184

Bender J, Wagner NJ (1996) Reversible shear thickening in monodisperse and bidisperse colloidal dispersions. J Rheol 40:899–916

Bertrand E, Bibette J, Schmitt V (2002) From shear thickening to shear-induced jamming. Phys Rev E 66:60401

Boersma WH, Baets PJM, Laven J, Stein HN (1991) Time-dependent behavior and wall slip in concentrated shear thickening dispersions. J Rheol 35:1093–1120

Bossis G, Brady JF (1989) The rheology of Brownian suspensions. J Chem Phys 91:1866–1874

Brown E, Jaeger HM (2009) Dynamic jamming point for shear thickening suspensions. Phys Rev Lett 103:086001

Brown E, Jaeger HM (2012) The role of dilation and confining stresses in shear thickening of dense suspensions. J Rheol 56:875–923

Cates ME, Haw MD, Holmes CB (2005) Dilatancy, jamming, and the physics of granulation. J Phys-Condens Mat 17:S2517–S2531

Cates ME, Wittmer JP, Bouchaud JP, Claudin P (1998) Jamming, force chains, and fragile matter. Phys Rev Lett 81:1841–1844

Chow MK, Zukoski CF (1995) Gap size and shear history dependencies in shear thickening of a suspension ordered at rest. J Rheol 39:15–32

Deboeuf A, Gauthier G, Martin J, Yurkovetsky Y, Morris JF (2009) Particle pressure in a sheared suspension: a bridge from osmosis to granular dilatancy. Phys Rev Lett 102:108301

D'Haene P, Mewis J, Fuller GG (1993) Scattering dichroism measurements of flow-induced structure of a shear thickening suspension. J Colloid Interf Sci 156:350–358

Fall A, Bertrand F, Ovarlez G, Bonn D (2012) Shear thickening of cornstarch suspensions. J Rheol 56:575–591

Fall A, Huang N, Bertrand F, Ovarlez G, Bonn D (2008) Shear thickening of cornstarch suspensions as a reentrant jamming transition. Phys Rev Lett 100:018301

Fall A, Lemaitre A, Bertrand F, Bonn D, Ovarlez G (2010) Shear thickening and migration in granular suspensions. Phys Rev Lett 105:268303

Fielding SM, Olmsted PD (2004) Spatiotemporal oscillations and rheochaos in a simple model of shear banding. Phys Rev Lett 92:084502

Fischer P, Wheeler EK, Fuller GG (2002) Shear-banding structure oriented in the vorticity direction observed for equimolar micellar solution. Rheol Acta 41:35–44

Foss DR, Brady JF (2000) Structure, diffusion and rheology of Brownian suspensions by Stokesian dynamics simulation. J Fluid Mech 407:167–200

Franks GV, Zhou ZW, Duin NJ, Boger DV (2000) Effect of interparticle forces on shear thickening of oxide suspensions. J Rheol 44:759–779

Frith WJ, Lips A (1995) The rheology of concentrated suspensions of deformable particles. Adv Colloid Interfac 61:161–189

Head DA, Ajdari A, Cates ME (2002) Rheological instability in a simple shear-thickening model. Europhys Lett 57:120–126

Isa L, Besseling R, Morozov AN, Poon WCK (2009) Velocity oscillations in microfluidic flows of concentrated colloidal suspensions. Phys Rev Lett 102:058302

Kalman DP, Rosen BA, Wagner NJ (2008) Effects of particle hardness on shear thickening colloidal suspension rheology. In: Co A, Leal LG, Colby RH, Giacomin AJ (eds) The XVth international congress on rheology, the society of rheology 80th annual meeting, pp 1408–1410

Kalyon DM (2005) Apparent slip and viscoplasticity of concentrated suspensions. J Rheol 49:621–640

Kim JW, Larsen RJ, Weitz DA (2007) Uniform nonspherical colloidal particles with tunable shapes. Adv Mater 19:2005

Kramb RC, Zhang R, Schweizer KS, Zukoski CF (2010) Glass formation and shear elasticity in dense suspensions of repulsive anisotropic particles. Phys Rev Lett 105:055702

Kramb RC, Zukoski CF (2011) Exploration of the volume fraction above which suspensions of spherical and weakly anisotropic colloid particles cannot flow. J Rheol 55:1085–1101

Kulkarni SD, Metzger B, Morris JF (2010) Particle-pressure-induced self-filtration in concentrated suspensions. Phys Rev E 82: 010402

Larsen RJ, Kim JW, Zukoski CF, Weitz DA (2010) Elasticity of dilatant particle suspensions during flow. Phys Rev E 81:011502

Laun HM, Hirsch G (1989) New laboratory tests to measure rheological properties of paper coatings in transient and steady-state flows. Rheol Acta 28:267–280

Laun HM, Bung R, Schmidt F (1991) Rheology of extremely shear thickening polymer dispersions (passively viscosity switching fluids). J Rheol 35:999

Laun HM (1994) Normal stresses in extremely shear thickening polymer dispersions. J Non-Newton Fluid 54:87–108

Lee YS, Wagner NJ (2003) Dynamic properties of shear thickening colloidal suspensions. Rheol Acta 42:199–208

Lee YS, Wetzel ED, Wagner NJ (2003) The ballistic impact characteristics of Kevlar (R) woven fabrics impregnated with a colloidal shear thickening fluid. J Mater Sci 38:2825–2833

Lee M, Alcoutlabi M, Magda JJ, Dibble C, Solomon MJ, Shi X, McKenna GB (2006) The effect of the shear-thickening transition of model colloidal spheres on the sign of N_1 and on the radial pressure profile in torsional shear flows. J Rheol 50:293–311

Lootens D, Van Damme H, Hebraud P (2003) Giant stress fluctuations at the jamming transition. Phys Rev Lett 90:178301

Lootens D, Van Damme H, Hemar Y, Hebraud P (2005) Dilatant flow of concentrated suspensions of rough particles. Phys Rev Lett 95:268302

Meeker SP, Bonnecaze RT, Cloitre M (2004) Slip and flow in pastes of soft particles: direct observation and rheology. J Rheol 48:1295–1320

Melrose JR, Ball RC (2004) Contact networks in continuously shear thickening colloids. J Rheol 48:961–978

Mills P, Snabre P (2009) Apparent viscosity and particle pressure of a concentrated suspension of non-Brownian hard spheres near the jamming transition. Eur Phys J E 30:309–316

Nakanishi H, Nagahiro S, Mitarai N (2012) Fluid dynamics of dilatant fluids. Phys Rev E 85:011401

Nakanishi H, Mitarai N (2011) Shear thickening oscillation in a dilatant fluid. J Phys Soc Jpn 80:033801

O'Brien VT, Mackay ME (2000) Stress components and shear thickening of concentrated hard sphere suspensions. Langmuir 16:7931–7938

Salmon J-B, Colin A, Roux D (2002) Dynamical behavior of a complex fluid near an out-of-equilibrium transition: approaching simple rheological chaos. Phys Rev E 66:031505

Waitukaitis SR, Jaeger HM (2012) Impact-activated solidification of dense suspensions via dynamic jamming fronts. Nature 487:205–209

Yilmazer U, Kalyon DM (1991) Dilatancy of concentrated suspensions with Newtonian matrices. Polym. Composite 12:226–232

Yoshimura AS, Prudhomme RK (1988) Wall slip effects on dynamic oscillatory measurements. J Rheol 32:575–584

Yoshimura AS, Prudhomme RK, Princen HM, Kiss AD (1987) A comparison of techniques for measuring yield stresses. J Rheol 31:699–710